Catalysis Science & Technology

Accepted Manuscript

ROYAL SOCIETY OF CHEMISTRY

www.rsc.org/catalysis

Catalysis Science & Technology RSCPublishing

ARTICLE

Toward enhanced conversion of model biogas mixtures: Parametric tuning and mechanistic study for ceria-zirconia supported nickel-cobalt catalyst

M. S. Aw,[a] I. G. Osojnik Črnivec[a] and A. Pintar[a,b]

Cite this: DOI: 10.1039/x0xx00000x

Received 00th January 2014
Accepted 00th January 2014

DOI: 10.1039/x0xx00000x

www.rsc.org/

This work underlines the parametric tuning and mechanistic study for ceria-zirconia (CeZr) supported bimetallic NiCo in methane dry reforming (MDR) with carbon dioxide. CeZr mixed oxides were calcined at three separate temperatures, i.e. 300, 350 and 400 ^{o}C. 1.5, 2.0, 2.5 and 3.0 wt. % NiCo were deposited onto CeZr support to assess their activity in MDR. Their physicochemical properties were characterized via XRD, FESEM, N_2 sorption, He pycnometry, TG-DSC, TPR and TPO. Results show that lower calcination temperature renders larger surface area in CeZr for more effective NiCo anchoring and particle dispersion. The optimum calcination temperature for CeZr was 350 ^{o}C, in which agglomeration-free morphology was identified. 2.5 wt. % emerged as the optimized loading parameter for NiCo deposition. This particular catalyst supported on CeZr calcined at 350 ^{o}C display the best performance for 20 h of MDR in terms of syngas yield (CO = 61 %, CO production rate = 11.1 mol/(g_{cat} h); H_2 = 38 %, H_2 production rate = 7.0 mol/(g_{cat} h)) and low carbon deposition (0.1 wt. %). Kinetic and mechanistic study infers that calcination temperature of CeZr support and adequate loading of NiCo are pivotal toward enhancing MDR activity.

1. Introduction

Carbon dioxide and methane are potent culprits for global warming – a serious environmental problem that has not been resolved to date. It is crucial to eliminate the rapidly increasing amount of these greenhouse gases, because they entrap large amounts of undesirable heat that disrupt the natural variability of climate and ecology.[1] A practical solution lies in methane dry reforming (MDR), in which this reaction encompasses both gases, and enables their conversion into syngas to generate renewable energy via gas-to-liquid (GTL) technology such as Fischer-Tropsch synthesis. Also, they are extensively applied in methanol manufacturing and hydrogenation for fuel production.[2] It is, at present, one of the most vital industrial processes for environmental waste handling and the valorization of CO_2 emissions. A major source of these two gases is derived from biogas, which is easily produced through anaerobic degradation of organic matter collected from aquatic or organic waste, soils from landfills, lagoons and animal excrete.[3] Applying current catalyst technology, it is feasible for the transformation of biogas through MDR according to the following chemical reaction:

$$CH_4 + CO_2 \leftrightarrow 2H_2 + 2CO \ (\Delta H^{o}_{298\ K} = +\ 247\ kJ/mol) \quad (1)$$

MDR consumes 1.6 times more energy than the steam reforming of methane.[4] However, its environmental benefits are more pronounced as it consumes CO_2, unlike the latter. In order to achieve high syngas output, a CH_4/CO_2 ratio of ideally 1:1 and a high reaction temperature are desirable. Moreover, it was concluded from our previous work that 750 ^{o}C and temperatures higher thereof are thermodynamically more favorable to drive the endothermic MDR equilibrium (eq. (1)) toward the right.[5]

It is crucial to design an economically feasible catalytic system. Unfortunately, noble metals tend to be precious but unaffordable for industrial mass purchase due to their rarity and extremely high price, despite their merits in promoting high syngas production, long stability and satisfactory low coking rates in MDR attributed to their corrosive-resistant nature.[6] Nevertheless, ample supply of cost effective Ni-based catalyst continues to emerge as a remarkable and economically viable catalytic system. The downside is they are highly sensitive to coke deposition, which obstructs their application for long-term industrial reforming. Devising a robust support is an attractive solution to rectify the current problems. Large specific surface area in a support with good chemical inertness and high oxidation stability are essential criteria to resist corrosion, overcome low catalyst utilization and decrease overall capital cost.[7] Excellent electron conductivity is also required because

electron migration and charge transfer process can occur more smoothly, since conductivity is directly related to redox properties of the support.[8] The support per se may create special interfacial sites, wherein reactions can proceed, intermediates or products can be stabilized, and interactions with reactants can occur smoothly in the catalytic cycle.[9] In recent research on novel supported catalysts, the exceptional properties of ceria (Ce), for example, high oxygen storage capacity could indirectly increase the dispersion of metallic active phases. The reason being good electron conductivity that is in ceria is capable of determining the ordering of cations and oxygen vacancies in the lattice, which in turn, improves the immobilization of metal nanoparticle on the surface. The interaction between catalyst nanoparticles and the support is electronic and involves charge transfer between them.[10] Ceria has been recognized as an effective promoter for Ni in hydrocarbon reforming reactions.[11] Meanwhile, another candidate, namely, zirconia (Zr), is capable of enhancing CO_2 adsorption on catalyst surface, because it contains oxygen vacancies that can be continually replenished by CO_2 during MDR as reported in literature.[12] The containment of CO_2 ultimately led to CO formation over Zr vacancies. Additionally, Mustu et al. had also claimed that Zr possesses good affinity to CO_2 adsorption, and is considered as a promising catalyst support for this reaction.[13] Moreover, using Zr as a dopant could improve the mechanical strength of support to facilitate catalysis.[14] Successful incorporation of Zr in Ce enables the formation of a highly tense crystalline lattice with numerous structural defects, that are known to increase the oxygen mobility within the crystalline structure. In this way, the adsorption of CO_2 increases considerably. We postulate, therefore, that CeZr is a promising bi-functional catalyst support (as confirmed by our previous results),[5b] signalling a new era of NiCo-based catalysts for MDR. Notwithstanding skilful techniques for the preparation of this supported catalyst, there remains uncertainty in the modulation for certain parameters, i.e. the optimal quantity of Ni and Co deposition, and the tuning of calcination temperature for CeZr support. This is because the variables pertaining to catalyst, such as its quantity and its support synthesis, to a great extent, were not sufficiently adjusted based on past protocols.

We herein explore the tuning of these variables: (i) the calcination temperature for the CeZr support, and (ii) the quantity of NiCo for loading, to identify the suitable parameter from a set range to obtain the best performing catalyst. In essence, calcination temperature plays a substantial role in the quality of the support, whereas the proper amount of catalyst loading (that is not too high or low) is vital to ensure sufficient catalytic active phase for stable activity and product yield, considering the fact that no other studies have been established; and thus far, this is the first. The appropriate calcination temperature to retain as high as possible the initial specific surface area of CeZr mixed oxide support, as well as to accommodate highly dispersed NiCo phase is necessary to be sought. Previously, CeZr was calcined at temperatures up to 800 °C, which resulted in abrupt and marked depletion of BET surface area in the support.[15] Also, higher loading range of NiCo, i.e. 6-18 wt. % that was employed before in our work had caused severe NiCo phase aggregation and particle sintering. Consequently, lower loading range of 1.5 to 3.0 wt. % was opted instead to prevent such undesirable occurrence. This work is an ongoing, cumulative continuation from our previous in MDR research based on CeZr/NiCo catalyst.[5b]

2. Results and discussion

2.1 Nanocrystalline structure of catalyst support

Fig. 1 displays the x-ray diffractograms for 1.5, 2.0, 2.5 and 3.0 wt. % NiCo catalysts loaded onto CeZr support calcined at 400 °C, showing signals that were detected in the XRD peaks. The Ce to Zr ratio is 4 : 1, and Ni to Co ratio is 2 : 3. By comparing this series to the diffractogram for pure ceria from the commercial batch with peaks arising at 2θ = 28.55, 32.80, 47.35, 56.35, 59.00, 69.65, 78.55, 78.95°, which shows XRD peaks of pure ceria correspond to its (111), (200), (220), (311), (222) and (400) crystal planes, it reveals well-developed reflections of cerium oxide (ICDD PDF No. 81-0792), space group *Fm3m*, with cubic fluorite (FCC) structure for comparison to signals in our catalysts. A curve of Δ2θ and several arrows were drawn in Fig. 1 to show the changes of position for the main signals from pure ceria. Shifting was seen for these characteristics peaks.[16] Apparently, the presence of Zr species distorted the original Ce nano-crystalline lattice. This also indicates that the interplanar crystal spacing of the support slightly differ from pure ceria. The partial substitution in Ce^{4+} (97 pm) by the smaller Zr^{4+} (84 pm) cations, however, did not give rise to tetragonal characteristics resembling that of ZrO_2 besides the face-centered-cubic (FCC) configuration. Ceria nano-crystalline phase was in fact retained. Furthermore, no evidence or traces of Ni or Co was observed in the diffracto-

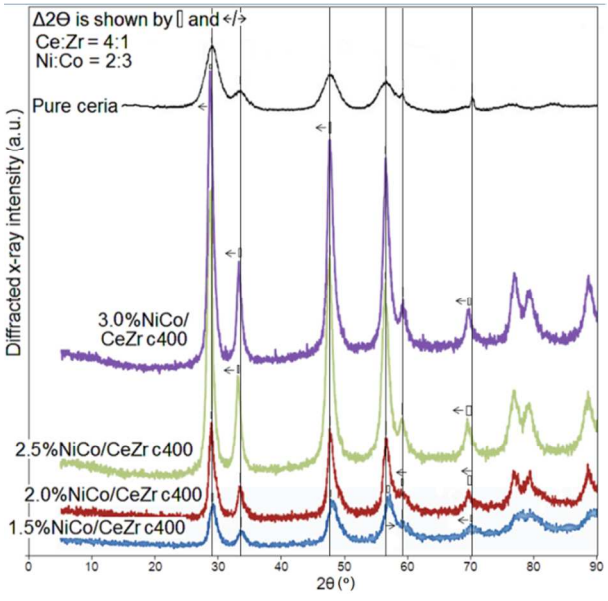

Fig. 1 XRD diffractogram showing spectra of 1.5, 2.0, 2.5 and 3.0 wt. % NiCo samples all loaded onto CeZr c400 supports.

grams of all samples, due to amorphous nature, or too low loading amount of these elements that was not sufficed for x-ray diffraction. Even with literature reporting 5 wt. %, not all NiCo metals can literally be inserted into the CeZr support, due to smaller Ni^{2+} (69 pm) cation size that is not compatible with Co^{2+} (75 pm) and Zr^{4+}. In our case, the maximum total NiCo loading is 3 wt. %. Up to this value, there is no rejection of Ni in its incorporation into the fluorite CeZr structure.[17] Because 1.5 and 2.0%NiCo/CeZr c400 samples contain less metals and thus are less dense, they scatter with lower intensity. Also, they have lower orientation in the lattice plane, and so the scattering angle has increased.[18] The crystallinity of all samples are the same, as reported in a previous paper, XRD profile of our catalyst matches precisely that of the XRD standard with a designated composition for $Ce_{0.75}Zr_{0.25}O_2$ (PDF standard 00-028-0271) for all observed characteristics peaks.[15] Furthermore, XRD and H_2-TPR measurements indicate properties resulting from a homogeneous solid solution and therefore phase segregation and amorphous nature of formed Ce and Zr oxides may be excluded.[15,19] However, with larger particles as in the higher NiCo loading and higher calcination temperature for the CeZr support, sharper peaks were observed. Different relative intensities could also be ascribed to the slight differences in their texture effects, different broadening of reflection lines, as well as from site inversion occupation. Due to non-distinguishable difference in the diffractogram for each of CeZr c300, c350 and c400 supports, only CeZr c400 was shown here in this work (due to data congestion). The rest consisting of CeZr support c300, c350 and c400, alongside 1.5-3.0%NiCo/CeZr c300 and 1.5-3.0%NiCo/CeZr c350 solids are included in the Supplementary Material, (ESI, Figs. S1-S3). The average crystallite size for these as-synthesized CeZr support was measured from the diffraction line using Scherrer's equation, giving rise to a mean value of 5.0 nm.

2.2 Textural properties of supports and supported catalysts

Table 1 exhibits the textural properties of the CeZr support and CeZr/NiCo catalyst. It is observed that the lower the calcination temperature, the greater the surface area of the support can be obtained; but conversely, pore diameter is lowered. 2.5% NiCo recorded the highest surface area for both c300 and c350 amongst all other loading values. Comparing the two, 2.5% NiCo with CeZr c350 catalyst provides the highest surface area, which is most favorable for the dispersion of active metal solids. 3.0% NiCo samples gave rise to pore size exceeding 10 nm. There is a negligible variation in the total pore volume of all samples. This proves that the changes in the calcination temperature, in other words, heat treatment on the catalyst supports have a minimal impact on it. Furthermore, no noticeable correlation can be found in their density values ranging from 5.3-6.5 g/cm^3. Skeletal density was measured in our work, wherein the volume measured excludes the inaccessible (closed) micropores. It is defined as the mass of a particle divided by its volume, excluding open and closed pores. Helium (He) gas quickly and thoroughly fill the minutest pore spaces in He gas pycnometer, as long as the void spaces are reachable for the gas molecules (but not the closed pores). As NiCo-loaded catalysts were featured in an unreduced, unactivated, oxidic state, and also because CeZr is more porous as a support (before Ni and Co solids were load on it), which involved the final step of thermal treatment for the preparation of the catalyst, skeletal density of the support was lower as seen in Table 1.[20] However, lower skeletal density which is more favorable for MDR is identified in CeZr c350 (outperforming c300 and c400 in terms of CeZr supports without NiCo solids); and as for the catalysts, the least dense ones are: 3.0%NiCo/CeZr c300, 2.0%NiCo/CeZr c400, 1.5%NiCo/CeZr c400 and 2.5%NiCo/CeZr c350. Furthermore, pore size analysis utilizing BJH pore size distribution and data discussion are elaborated in Supplementary Information.

Table 1 Textural properties of prepared supports and catalysts (BET surface area (S_{BET}), total pore volume (V_{TP}), average pore diameter (d_p) and skeletal density (ρ_s)).

Sample	S_{BET} (m^2/g)	V_{TP} (cm^3/g)	d_p (nm)	ρ_s (g/cm^3)
CeZr c300	127.1	0.82	6.5	5.66
CeZr c350	117.9	0.81	7.1	5.39
CeZr c400	108.6	0.81	8.7	5.51
1.5%NiCo/CeZrc300	43.2	0.84	8.8	6.49
2.0%NiCo/CeZrc300	40.3	0.85	9.0	6.49
2.5%NiCo/CeZrc300	48.3	0.85	6.5	6.47
3.0%NiCo/CeZrc300	44.6	0.81	10.8	5.32
1.5%NiCo/CeZrc350	35.6	0.85	8.8	6.49
2.0%NiCo/CeZrc350	38.8	0.84	8.9	6.38
2.5%NiCo/CeZrc350	55.3	0.84	7.4	6.32
3.0%NiCo/CeZrc350	53.3	0.85	10.8	6.44
1.5%NiCo/CeZrc400	45.6	0.84	11.0	6.16
2.0%NiCo/CeZrc400	52.5	0.83	9.1	6.04
2.5%NiCo/CeZrc400	41.5	0.84	6.5	6.36
3.0%NiCo/CeZrc400	50.1	0.85	10.1	6.49

2.3 Reducibility of the as-synthesized supported catalysts

Reduction properties of NiCo catalyst supported on CeZr metal oxides, based on TPR data as depicted in Fig. 2, show that the reduction peaks are similar for 1.5, 2.0 and 2.5%NiCo/CeZr c400. In particular, 300 ^oC is the lower temperature whereby 1.5%NiCo/CeZr c400 was reduced, i.e. earlier than 2.0 to 3.0 wt. % NiCo/CeZr c400. The onset reduction temperatures for 2.5%NiCo/CeZr c400 and 2.0%NiCo/CeZr c400 occurred at 324 and 350 ^oC, respectively. The reduction below 100 °C is ascribed to surface hydration, because as the catalyst is reduced, the catalyst becomes smaller, surface area increases, and thus the reduced state has a higher affinity to water at this low temperature. Also, the reduction could also be due to high surface area from the support with an exposure of multiple active crystal planes, i.e. (100), (110) and (200) of ceria formed from surface reduction of the most stable cubic space group (111) planes that are much easier to reduce at lower temperatures.[21] There was an initial peak of reduction at ca. 100 ^oC for 3.0%NiCo/CeZr c400, but it levelled off until the

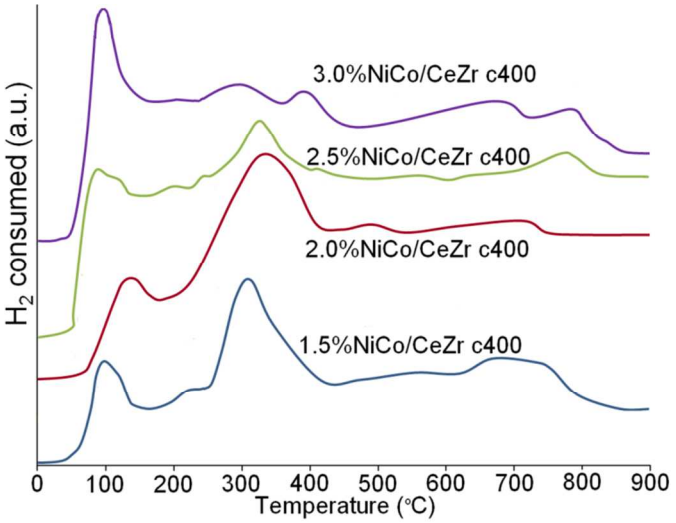

Fig. 2 H_2-TPR profiles depicting H_2 consumed in arbitrary units as a function of temperature for different loading amount of NiCo (1.5, 2.0, 2.5 and 3.0 wt. %) with CeZr support calcined at 400 °C.

temperature reached 280 °C. Likewise, the same trend occurred for 1.5%NiCo/CeZr c400, 2.0%NiCo/CeZr c400 and 2.5%NiCo/CeZr c400, respectively. The H_2 consumed from RT until 500 °C for these catalysts correspond to the reduction of Co^{3+} to Co^{2+} species. 1.5%NiCo sample was relatively the least stable amongst all, because its decomposition started the earliest. The shouldered reduction curves for all samples extending from 400 to 620 °C encompass the reduction of NiO and surface ceria. The higher temperature reduction peak which occurred at temperatures beyond 650 °C, as depicted in all samples, exhibited the complete reduction of Ni^{2+} from NiO phase to metallic Ni^0 species and Co^{2+} to metallic Co^0 formation.[22] Surprisingly, the reduction of bulk Co_3O_4 species which supposedly occurs at 550 °C was not detected. It is inferred that an alloy formation of NiCo hindered the bulk reduction as such, and that there exists a synergetic effect between Ni and Co species that increased the resistance of both metals. The 1.5%NiCo and 2.0%NiCo samples also displayed a third peak, at 767 and 724 °C, respectively. This is assigned to the reduction of bulk ceria of their catalyst support.[23] It was evident that the reductive peaks of bulk ceria shifted to higher temperature as compared to pure ceria, suggesting increased thermal stability due to resultant doping of Zr in this mixed oxide support that caused a distortion in the lattice, albeit the lattice not conformed to monoclinic state of Zr. This is in agreement with our previous results from XRD analysis. Interestingly, the area of H_2 consumption of bulk ceria for 2.5%NiCo/CeZr c400 was greater than the lower metal loading samples, but slightly less of that for 3.0%NiCo/CeZr, indicating substantial reduction which comprises not only the reduction of surface per se, but also bulk ceria. Moreover, its reduction could happen more readily than 2.0%NiCo/CeZr, as its signal was detected at a lower temperature, rendering this catalyst more advantageous than the others.

2.4 Methane dry reforming activity test

2.4.1 Evaluation on 1.5-3.0 wt. % NiCo catalysts with support calcined at 300 °C. Fig. 3 shows the syngas production and CH_4/CO_2 conversion profiles for (a) 1.5%NiCo/CeZr c300, and (b) 3.0%NiCo/CeZr c300 catalysts after 20 h MDR reaction. All graphs exhibit no deactivation of catalyst and negligible decline in the selectivity of H_2 gas, implying a sustained MDR reaction process for 20 h. The activity patterns in the catalysts did not differ by a large extent, only the quantity variation that is more distinctly observed. In Fig. 3a, the syngas yields and CH_4/CO_2 conversions are low, due to low loading of catalyst. However, the activity is stable. Likewise, Fig. 3b shows stable behavior but with high product yield, i.e. 50 % for CO and 39 % for H_2, so as for CH_4/CO_2 conversion, i.e. 87 % for CO_2 and 71 % for CH_4.

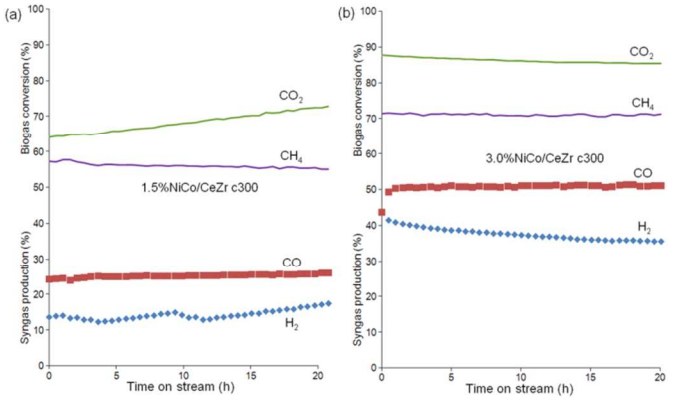

Fig. 3 Syngas production and CH_4/CO_2 conversion profiles after 20 h MDR reaction for (a) 1.5%NiCo/CeZr c300, (b) 3.0%NiCo/CeZr c300 catalysts.

2.4.2 Evaluation on 1.5-3.0 wt. % NiCo catalysts with support calcined at 350 °C. Fig. 4 shows the syngas production and CH_4/CO_2 conversion profiles after 20 h MDR reaction for (a) 1.5%NiCo/CeZr c350, and (b) 3.0%NiCo/CeZr c350 metal solids. CH_4 conversion was noticeably and consistently lower than CO_2 due to pronounced reverse water gas-shift (RWGS) side reaction ($CO_2 + H_2 \rightarrow H_2O + CO$) occurring concurrently with MDR. Meanwhile, Fig. 4b displays a sudden overshoot in CO yield in the first 4 h, which then subsided before it stabilized and remained as such throughout the process. The reason is that small particles of NiCo induce excellent CH_4 decomposition at the start of the MDR; the cracking of CH_x species provides surface carbon for further oxidation to CO, so as for reverse Boudouard reaction ($CO_2 + C \rightarrow 2CO$) that induces carbon gasification to occur as it favors small particles and the process is structure-sensitive.[24] The temporary decrease of catalytic activity in the short amount of time perceived in both 1.5%NiCo and 3.0%NiCo samples is due to the fact that by-products were formed as a result of the simultaneous secondary reactions, especially at such high temperature of 750 °C, which had also contributed to their catalytic deactivation. Fig. 4b shows the higher syngas production and CH_4/CO_2 conversion which proceeded more

stable than the other catalyst in Fig. 4a, showing no signs of deactivation unlike the latter; where H_2 selectivity severely dropped as shown in Fig. 4a, viz. H_2 markedly decreased from 43 to 12 % albeit it plateaued after t = 7 h at that very low level. This is due to the much lower amount of NiCo, resulting in the lower number of catalytic sites on the 1.5%NiCo metal solids. Other contributing factors include vast sintering of NiCo metal solids. It is proposed that the well-dispersed NiCo nanoparticles facilitated their oxides to form more interfacial contact with the support, which might have provided more active sites. Therefore, it can be said that more NiCo alloys are present in the more highly dispersed form in Fig. 4b than in Fig. 4a. Based on Table 1 and Fig. 2 previously, it can be seen that the textural properties of CeZr, such as high surface area, regular and small size of the support calcined at 350 °C are manifested in Fig. 4a, wherein it is hypothesized that Ni and Co in nanocrystalline structure provide, at this relatively low temperature of calcination, effectively interspersed active metals.

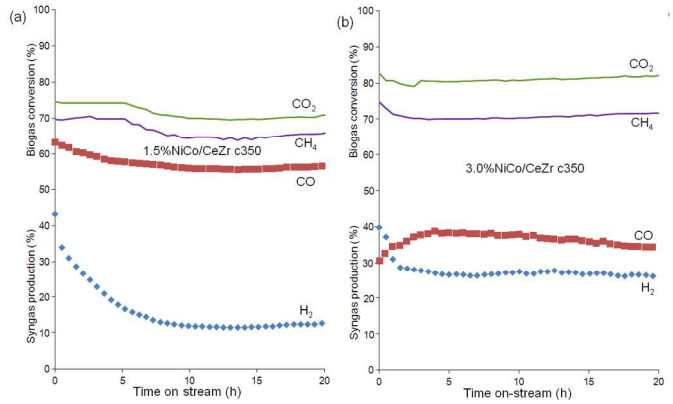

Fig. 4 Syngas production and CH_4/CO_2 conversion profiles after 20 h MDR reaction for (a) 1.5%NiCo/CeZr c350, (b) 3.0%NiCo/CeZr c350 catalysts.

2.4.3 Evaluation on 1.5-3.0 wt. % NiCo catalysts with support calcined at 400 °C. Fig. 5 shows the syngas production and CH_4/CO_2 conversion profiles after 20 h MDR reaction for (a) 1.5%NiCo/CeZr c400, and (b) 3.0%NiCo/CeZr c400. Comparing Fig. 5a and 5b, there is a similarly larger conversion for CH_4/CO_2 in 1.5%NiCo/CeZr c400 and 3.0%NiCo/CeZr c400 samples. However, the drop in conversion is significantly low for the latter. Deactivation of catalyst in Fig. 5a was extremely pronounced as there was a tremendous drop in H_2 production; and so, toward t = 13 h, almost no measurable activity can be described, because extensive coke formation had blocked the catalyst active sites. In Fig. 5b, conversely, the decline in syngas production is not as obvious, in which CO decreased from 50 to 44 %; whereas H_2 plummeted from an initial value of 41 to 30 %. This can be explained by the corrosive CO interaction with bimetallic NiCo, bringing about changes on the metal particle size and subsequently depleting the catalyst amount from the support surface, eventually causing catalyst loss and deactivation.[25] The difference in CH_4/CO_2 conversion is relatively much less than syngas production (0 to 10 %), indicating a disproportion from

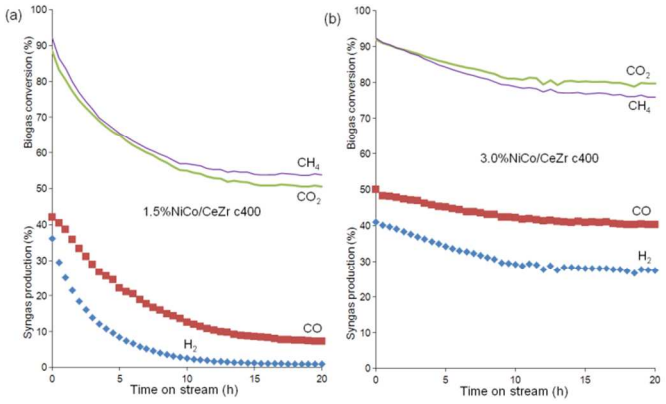

Fig. 5 Syngas production and CH_4/CO_2 conversion profiles after 20 h MDR reaction for (a) 1.5%NiCo/CeZr c400, (b) 3.0%NiCo/CeZr c400 catalysts.

the CH_4 cracking to the H_2 reaction process, and CO_2 dissociation to CO from the MDR process, considering their equimolar feed stream. This implies side reactions were indeed at play.

2.5 Production of syngas and catalytic turnover in MDR

Regarding the activity of examined solids, the specific reaction rate was measured in terms of production rates of H_2 and CO as listed in Table 2. Results show that 2.5 and 3.0% c300 samples, together with 2.5%NiCo/CeZr c350 produced H_2 at the highest level (>7 mol/(g_{cat} h)), inferring highest number of active sites present. Not only the nature of metal but taking into consideration their surface arrangement, are rate constants as a function of sites coverage. CO production rate is the highest for 3%NiCo/CeZr c350 solid. However, the H_2/CO ratio is then substantially lower. Quantitative relationship between improvements and the structure of catalyst can be distinguished by the variation in the rate for all catalysts as seen in Table 2. Normalized rate per unit active sites vary for each catalyst, showing the impact of tuning on the structure of catalyst by two important parameters indeed, viz. calcination temperature and catalyst loading amount. The limiting factors that caused the destabilization, and thus lowered production of syngas as shown in Fig. 4a and Fig. 5a–b is: low contact time of 0.6 s that hindered the interaction between the oxide support and the active metallic phase, and coking. Nevertheless, some decrease are negligible, especially in 2.5% and 3.0%NiCo loading on all supports (for 2.0%NiCo and 2.5%NiCo loaded on CeZr catalysts calcined from 300-400 °C, refer to Fig. S6, Supplementary Information). This is because more Ni and Co are proposed to be close to each other and formed alloys as their precursors were mixed in the sequential deposition precipitation method as previously mentioned in experimental preparations.[26] Moreover, although CH_4 was activated through the donation of σ-electrons of a C-H bond to empty *d*-orbitals in Ni species, coking extent could be reduced via CH_4 disproportion by the increased electron density of the active

metal.

2.6 Kinetics and mechanistic aspect of MDR over CeZr/NiCo

Since MDR results are influenced by NiCo and CeZr surface structure as shown previously, likewise, reaction mechanism changes with surface nature. In our case, reaction kinetics has to be understood first. Before tentative explanations could be put forth to elucidate the kinetic coupling of elementary steps, assumptions were made, such as: a one-dimensional model was used for our fixed-bed reactor with constant flow, isothermally at uniform pressure and uniform rate for co-reactant feed CO_2; MDR occurred under steady state conditions; partial pressure and molar rates of both reactants equal unity; there could be possible inhibition of reactant conversion from products; the main oxidizer is OH∗; and that all steps involving OH∗ are quasi-equilibrated.[27] Scheme 1 provides a simplified visual summarizing the proposed elementary steps, whereby CH_4/CO_2 underwent catalytic conversion into syngas via our as-prepared CeZr/NiCo in the MDR, alongside RWGS which is the major accompanying side-reaction. In this catalytic process, we propose that for the MDR catalytic cycles to turnover, firstly, CH_4 cracked via pyrolysis ($CH_4 \rightarrow C* \rightarrow CO*$). This produces C∗ radical on the catalyst surface that was later oxidized by OH∗ to CO∗, where carbon oxidation occurs via OH∗. Meanwhile, CO_2 adsorbed on the surface, and its activation happened because of H∗ radicals, based on $CO*_2 + H* \rightarrow CO* + OH*$ (eq. (2)). The CO_2 decomposition process ($CO*_2 + * \rightarrow CO* + O*$) that occurred simultaneously with the favorable process eq. (2) was considered negligible under our conditions, in agreement with literature.[28] Consequently, the oxidizer OH∗ was obtained directly from eq. (2). A small amount of the OH∗ reacted with H∗, producing H_2O, evidencing the non-ideal MDR state (i.e. not completely "dry" reforming), since water was partially formed. In other words, the RWGS side-reaction occurred, which coincidentally, elucidates the remarkably higher yield of CO over H_2 in the syngas production (as seen previously in Figs. 3-5), since it is thermodynamically favored at higher temperatures. Hence, we would presume that the steps involving the co-reactant turned out to be quasi-equilibrated; and the CH_3* dehydrogenation step ($CH_3* + * \rightarrow CH_2* + H*$) is deemed the rate determining step, gradually dissociating itself to $CH_2* \rightarrow CH*$, with the break-up of a H∗ radical during each elementary step from its hydrocarbon species. H∗ that was liberated would either combine with another of its own to form H_2 gas molecules on the resultant H_2-rich surface; or alternatively, reacts with OH∗ to produce undesirable water molecules. That said, however, the purpose of the co-reactant (CO_2) is to provide the OH∗ needed for C∗ oxidation; and that all steps involving OH∗ would turn out to be quasi-equilibrated.[29] This is because at such high MDR temperature, OH∗ is not likely to exist anymore (especially above 500 °C), as no branch of acidity is permissible; even if so, only extremely loose acidity could be anticipated. Other than that, one could also argue that CeZr support plays a significant role in CO_2 dissociation and induces enhanced redox process through O_2 contribution from ceria for C∗ oxidation. This

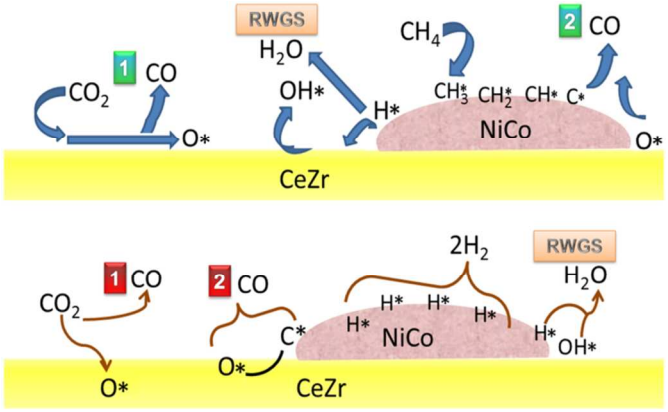

Scheme 1 Schematic diagram illustrating the elementary steps pertaining to the dissociation of CO_2 to form CO, storage of O∗ formation of CO from O∗ and C∗ which was sourced from methane, as well as the undesirable by-production of water due to RWGS side-reaction in the MDR.

reasoning was affirmed by the high O_2 storage capability of our ceria (ca. 60 %) and ca. 70 % reducibility of our CeZr support as reported in our previous paper.[15] Regardless, these hypotheses remain to be confirmed by in situ spectroscopic techniques in the near future.[30] Additionally, reaction tests involving RWGS side reactions, such as the difference in selectivity for water, and therefore, the achieved selectivity for RWGS due to unwanted production of water, its level and the quasi-equilibrium state of the reaction, had also been studied and discussed extensively in our previous work.[5c,15,19]

2.7 Coking analysis for spent catalysts post-MDR

2.7.1 FESEM. Fig. 6 displays the morphology of the fresh CeZr support before MDR reaction for comparison to post-MDR. It is observed in Fig. 6a that crystalline CeZr comprises nano-powdered porous structure, whereby sparsely aggregated surface is visibly seen. It is compact, crack-free and consistent throughout the surface. This is attributed to the hydrothermal synthesis process, because the nucleation growth of CeZr crystals could occur in a controlled manner. Agglomeration of the mixed oxides was also prevented due to short aging time (only 3.3 h) and low calcined temperature (350 °C). Fig. 6b shows the deposited NiCo catalyst in the form of flat, thin nanoporous sheets, measuring at 550-850 nm × 20 nm, which are almost two-dimensional-like (2D). Presumably, Ni- and Co-oxides were incorporated in the Ce and Zr oxides matrix and a continuous lattice fringe at the boundary with distinct edges exists. The metals in thin sheets do not show signs of large Ni- and Co-oxide particles nor agglomeration. Instead, with its wide exposed surface, they were embedded deep in the support. It is important to note that at the start of MDR, the catalyst surface was carbon-free. This is because even with any pre-formed or existing carbon during reduction, it is eliminated through the inverse Boudouard reaction with CO_2 from reactant mixture. Fig. 6c shows strings of ultra-fine filamentous carbon nanotubes formed on the spent catalyst post-MDR, with visible strands as long as 1.5 to 2.0 μm with 65 to 120 nm thickness

seen. Although this type of carbon was reported to be the most detrimental, the catalyst support was not disintegrated, as verified by the retained CeZr structure which can be visibly seen. It is expected that no decrease in activity would result from this type of carbon as mentioned in literature such as that of the encapsulating type. Likewise, other groups reported similar carbon with such structures over Ni-based catalysts, some diameter in the range of 50-200 nm. These carbon filaments are estimated to be 30-200 nm in width. They consisted typically of graphene layers oriented in certain manner relative to the axis forming 'herring-bone' or 'platet' or multiwall carbon nanotubes (angle α = 15-45, 90 or 0°).[31] Also from Fig. 6c, there was a fairly low amount of filamentous carbon, suggesting that merely some particles were large enough to produce these structures. This inferred that catalysts were stable during the reaction and the coke produced was not harmful to the catalyst. A minimum metal particle diameter of approximately 6 nm is required to form filamentous carbon, implying that partial existing amount of our metal solids are of that size.[32]

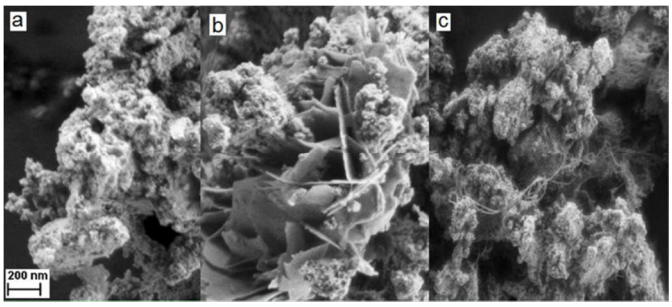

Fig. 6 (a) Catalyst support: Surface morphology of ceria-zirconia mixed oxides calcined at 350 °C for 4 h; (b) Fresh catalyst: 2.5 wt. % NiCo loaded onto it post-calcination at 650 °C for 4 h; (c) Spent catalyst with the formation of carbon nanotubes visible on the surface after methane dry reforming (MDR) reaction at 750 °C.

2.7.2 TPO analysis. Fig. 7 displays the graph correlating the extent of coking (wt. %) to the spent catalysts post-20 h MDR calcined at 300, 350 and 400 °C, respectively, with varied NiCo loading (from 1.5 to 3.0 wt. %). Coking was most severe for the catalyst calcined at 400 °C, in which a direct linear correlation of coking with respect to calcination temperature is detected for 1.5, 2.0 and 2.5 wt. % NiCo. This is because higher thermal treatment resulted in the reduction of CeZr surface area, causing agglomeration.[33] Coking was significantly low (0.09 to 1.12 wt. %) due to lesser amount of NiCo particles which lowered the likelihood of metal sintering, and also because of increased thermal resistance from Zr species. 2.5 wt. % NiCo loading shows the best graph in this regard. The reason coking is considerably low is that Zr imparts higher stability in the catalyst by inhibiting carbon formation. Because the Ni and Co clusters are in the oxide forms, they could also contribute to the lack of carbon nanotubes. The low coking substantiates the low deactivation as shown in the activity test previously (Figs. 4–6). Results reflect that there is no direct relation between catalytic activity and the amount of surface carbon measured.

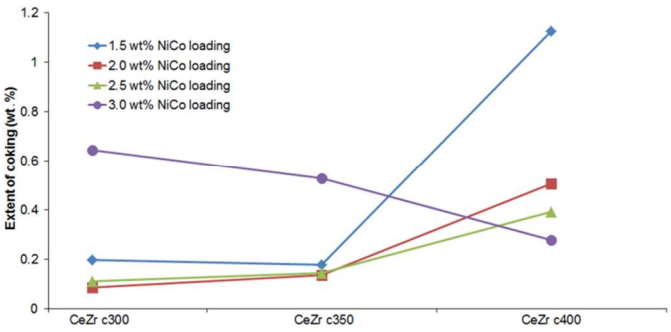

Fig. 7 TPO analysis showing the graph of the extent of coking (wt. %) versus the calcination temperature of the catalyst in the range of 300–400 °C, with varied NiCo loading (from 1.5 to 3.0 wt. %).

To this end, it is interesting to discuss the fact that changing the calcination temperature from 300 to 400°C has a so dramatic effect on the MDR activity, moderately on the coking extent, while the reaction itself at 750 °C seems not to affect severely the catalyst stability. This is so because the support underwent ~8 % increase in surface area as the calcination temperature was decreased from 400 to 300 °C, that led to higher dispersion of Ni and Co crystallites during their loading in the deposition precipitation step, which contributed to the dramatic effect. The samples calcined at lower temperature are more structurally protected, because of lower degree of sintering, smaller particle size, and better anchoring of Ni and Co clusters on the CeZr support. The migration and subsequent immobilization of Ni and Co active metallic phase most likely occurred in the reductive atmosphere during the H_2 reduction step before the start of the MDR activity test. For the supported catalysts, since the textural properties of them all do not differ substantially (Table 1), the reaction stability was therefore not severely affected. A similar outcome was also evidenced in literature, whereby Bitter et al. reported Pt/ZrO_2 as an active catalyst for CO_2/CH_4 reforming, but the catalyst is sensitive to the calcination temperature that impacted the activity due to Pt metal area loss at high calcination temperatures causing a significant drop in activity.[12a]

3. Experimental

3.1 Preparation of support for catalyst

Ceria-zirconia support (CeO_2-ZrO_2) (wt. ratio = 4 : 1, denoted as CeZr) was prepared via hydrothermal synthesis with ethylene glycol (EG),[15,19] wherein the synthesis procedure of ceria spheres reported by Liang et al. was followed but parameters modified to cater to our case.[34] 11 g of cerium (III) nitrate hexahydrate (Fluka, p.a.) and 3 g zirconium (IV) oxynitrate hydrate precursors (Sigma Aldrich, >99 % purity) were mixed and stirred vigorously in 14 mL Milli-Q warm water. The solution was added into 14 mL propionic acid

(Merck, >99 % purity) and 210 mL EG (Merck, >99 % purity) and mixed well, followed by 3.3 h-long aging in Teflon-clad stainless steel autoclaves at 180 °C. Next, in order to separate the solids from esterified solution in the mixed suspension, centrifugation at 8950 rpm in a 15 min-long cycle at room temperature (RT) was carried out. The precipitates were copiously washed with water and ethanol, before centrifuged again to eliminate the supernatants under the same conditions. The solids were dried overnight and then oven-calcined at 300, 350 and 400 °C in air for 4 h, with a heating ramp of 2 °C/min.

3.2 Preparation of catalyst

In order to deposit Ni and Co metals into CeZr mixed oxide support, firstly, 2 g Ni and 3 g Co nitrates precursors (Merck, p.a.) with Ni : Co = 40 : 60 w/w % were mixed with 33 g CeZr nano-crystalline powder and 27 g urea (Merck, p.a.) in a solution to produce 3 wt. % NiCo-contained catalyst. 1.5, 2, 2.5 wt. % of NiCo deposition onto the CeZr support calcined at the aforementioned three separate temperatures were also prepared accordingly. Deposition precipitation occurred via hydrolysis of 0.3 M urea at 90 °C for 22 h under reflux conditions. The reason for selecting this method is that there is a better control of CeZr porous structure and NiCo anchoring for its deposition as found in our previous work.[15] The pH of the aqueous suspension was increased in a gradual, controlled fashion upon a few drops of 65 % nitric acid (Merck, p.a.) at the start. The suspended solid matter was later separated from the liquid mixture by filtration. The solids were copiously rinsed with Milli-Q water and ethanol, before being oven-dried for 24 h at 70 °C. The final step was to thermally stabilize the catalyst by calcination in air at 650 °C for 4 h. The final as-prepared CeZr supported NiCo catalysts were ground into fine powder with agate mortar and pestle (Sigma-Aldrich).

3.3 Physicochemical characterization of supported catalyst

Catalysts were characterized by several techniques, namely, X-ray diffraction, XRD (X'pert Pro by PANalytical diffractometer), FESEM microscopy (Supra 35 VP), He pycnometry (AccuPyc II 1340 Gas Displacement Density Analyzer by Micromeritics) for skeletal density measurement, H_2-temperature programmed reduction (TPR) and temperature programmed-air oxidation (TPO), in order to probe their structural and textural properties. Experiments were further described in detail in Supplementary Information (Section S1). Additionally, TG-DSC analysis was conducted and its experimental, results and discussion were included in Supplementary.

3.4 Activity test for MDR

Before the as-prepared catalysts were tested for MDR, the powdered samples were reduced in a 20 % H_2/N_2 gas atmosphere at a flow rate of 50 NmL/min. Samples were heated from RT to 750 °C with a 10 °C/min ramp and held isothermally at 750 °C that lasted for 1 h. Upon reduction in H_2, an undiluted equimolar of gaseous CH_4/CO_2 reactants with a constant flow of 50 NmL/min each was fed into the reactor. Activity testing was carried out in a MicroActivity Reference Unit (PID Eng&Tech, Madrid, Spain), which is an automated and computer-regulated system containing a tubular fixed-bed continuous-flow quartz reactor (I.D. = 10 mm). Absolute operating pressure was set at a constant value of 1.2 bar throughout the process. 500 mg catalyst was weighed, uniformly mixed with 2833 mg of SiC buffer (0.2 mm wide, 0.5 mm long, density = 3.19 cm^3/g, S_{BET} = 0.03 m^2/g), and fixed between two quartz wool flocks for uniform heating throughout the bed inside the reactor (WHSV = 12 L/(g_{cat} h), corresponding to a residence time of gas phase = 0.6 s). A K-type Inconel thermocouple was positioned at the center of the catalyst bed for accurate temperature acquisition during the isothermal MDR process. Gases leaving the reactor were fed through a heated capillary (1/8 in. at 200 °C) to the GC (7890A, Agilent Technologies). Data were recorded every 30 min for 20 h for online analysis of quantitative and qualitative composition of discharged gases from the reactor outlet stream.

4. Conclusions

XRD shows the introduction of Zr species has led to extra force that increased the lattice strain of ceria. The high lattice strain from the ceria-rich support was reflected in FESEM as seen in the crystal defects, surface and edge effects. The average crystalline size for the CeZr support estimated according to Scherrer's equation equals to 5.0 nm. Results show that ceria-zirconia support calcined at 300 °C preserves the highest surface area. However, the same support calcined at 350 °C offers sufficiently large surface area for excellent dispersion of NiCo. This support that was deposited with 2.5 wt. % NiCo rendered the least amount of coking post-MDR reaction of all samples, reflecting its effectiveness for enhanced MDR activity, as well as minimal metal sintering. The reaction mechanism is elucidated by methane pyrolysis and carbon oxidation by OH∗ ($CH_4 \rightarrow C* \rightarrow CO*$), and it is proposed that CO_2 is the provider for the main oxidizer, OH∗ radical. Methane activation is suggested to be rate-determining for our MDR. Although this catalyst 2.5%NiCo/CeZr c350 does not give rise to the highest syngas production, however, its turnover rate of 7.0 mol/(g_{cat} h) (H_2) to 11.1 mol/(g_{cat} h) (CO_2) offers the closest H_2/CO ratio to 1. All CH_4/CO_2 conversion curves follow the same traits over the 20 h screening. In most case studies, CO_2 conversion is greater but there is no stark contrast. CeZr c350/2.5 wt. % NiCo catalyst is the most highly active and stable. It holds the most potential to produce adequate active metal sites for high syngas production and sustained catalytic activity in the MDR test. In conclusion, the two factors are confirmed as significant parameters toward enhancing syngas production and the tuning of these variables tender beneficial insights in synthesizing the best NiCo catalyst on CeZr support.

Acknowledgements

The authors gratefully acknowledge the financial support of the Ministry of Education, Science and Sport of the Republic of Slovenia through Research program P2-0150. The financial

support for the postdoctoral fellowship (M. S. Aw) offered by the National Institute of Chemistry, Ljubljana, Slovenia is gratefully acknowledged.

Notes and references

[a] Laboratory for Environmental Sciences and Engineering, National Institute of Chemistry, Hajdrihova 19, P. O. Box 660, SI-1001 Ljubljana, Slovenia

[b] Centre of Excellence "Low Carbon Technologies", Hajdrihova 19, SI-1001 Ljubljana, Slovenia

† Electronic Supplementary Information (ESI) available: [details of physicochemical characterization methods, results and discussion for pore size distribution, additional XRD diffractograms, TG-DSC curves of as-synthesized catalysts and further activity tests]. See DOI: 10.1039/b000000x/

1 (*a)* S. L. Yao, M. Nakayama and E. Suzuki, *Energy Fuels*, 2001, **15**, 1295; *(b)* Sk. Mahammadunnisa, P. Manoj Kumar Reddy, B. Ramaraju and Ch. Subrahmanyam, *Energy Fuels*, 2013, **27**, 4441.

2 (*a)* V. M. Gonzalez-Delacruz, R. Pereniguez, F. Temero, J. P. Holgado and A. Caballero, *ACS Catal.*, 2011, **1**, 82; *(b)* N. Wang, K. Shen, L. Huang, X. Yu, W. Qian and W. Chu, *ACS Catal.*, 2013, **3**, 1638; *(c)* G. A. Olah; G. K. Surya Prakash; A. Goeppert; M. Czaun and T. Mathew, *J. Am. Chem. Soc.*, 2013, **135**, 10030.

3 *(a)* S. Zhang, S. Muratsugu, N. Ishiguro and M. Tada, *ACS Catal.,*2013, **3**, 1855; *(b)* M. De Falco, G. Iaquaniello and G. Centi, in *CO_2: A Valuable Source of Carbon*, 1st ed.; R. Navarro, B. Pawelec, M. C. Alvarez-Galvan, R. Guil-Lopez, S. Al-Sayari and J. L. G. Fierro, Eds.; *Springer-Verlag: London*, 2013, **16**, 45; *(c)* W. M. Budzianowsk, *Int. J. Chem. Reactor Eng.,* 2010, **8**, Article A156.

4 *(a)* C. Papadopoulou, H. Matralis and X. Verykios, in: *Catalysis for Alternative Energy Generation,* 1st ed.; L. Guczi and A. Erdohelyi, Eds.; *Springer: New York*, 2012; **Chapter 3**, 57; (*b*) H. R. Gurav, R. Bobade, V. Lakshmi Das and S. Chilukuri, *Indian J. Chem.,* 2012, **51A**, 1339; *(c)* M. K. Nikoo and N. A. S. Amin, *Fuel Process.Technol.,* 2011, **92**, 678.

5 (*a*) H.-W. Chen, C.-Y. Wang, C.-H. Yu, L.-T. Tseng and P.-H. Liao, *Catal. Today*, 2004, **97**, 173; (*b*) P. Djinović, I. G. Osojnik Črnivec, J. Batista, J. Levec and A. Pintar, *Chem. Eng. Process*, 2011, **50**, 1054; *(c)* P. Djinović, J. Batista and A. Pintar, *Int. J. Hydrogen Energy,* 2012, **37**, 2699.

6 (*a)* B. Nematollahi, M. Rezaei and M. Khajenoori, *Int. J. Hydrogen Energy,* 2011, **36**, 2969; (*b*) M. Ocsachoque, F. Pompeo and G. Gonzalez, *Catal. Today,* 2011, **172**, 226.

7 (*a*) C. E. Daza, J. Gallego, F. Mondragon, S. Moreno and R. Molina, *Fuel,* 2010, **89**, 592; *(b)* M. Garcia-Dieguez, E. Finocchio, M. A. Larrubia, L. J. Alemany and G. Busca, *J. Catal*., 2010, **274**, 11.

8 S. Desinan, M. Miyayama and E. Traversa*, Nanostructured ceria-zirconia as a promising anode component for IT-SOFC: synthesis and characterization,* 210th ECS Meeting, Abstract #1742, 2006, copyright ECS.

9 O. Gamba, S. Moreno and R. Molina, *Int. J. Hydrogen Energy,* 2011, **36**, 1540.

10 *(a)* S. Damyanova and J. M. C. Bueno, *Appl. Catal. A*: *Gen*., 2003, **253**, 135-150; *(b)* R. Wang, H. Xu, X. Liu, Q. Ge and W. Li, *Appl. Catal. A: Gen*., 2006, **305**, 204-210.

11 S. C. Dantas, J. C. Escritori, R. R. Soares and C. E. Hori, *Chem. Eng. J.,* 2010, **156**, 380.

12 *(a)* J. H. Bitter, K. Seshan and J. A. Lercher, *J. Catal.,* 1997, **171**, 279-286; *(b)* A. M. Efstathiou, A. Kladi, V. A. Tsipouriari and X. E. Verykios, *J. Catal.*, 1996, **158**, 64-75; *(c)* S. Damyanova, B. Pawelec, K. Arishtirova, M. V. Martinez Huerta and J. L. G. Fierro, *Appl. Catal. B: Environ*., 2009, **89**, 149-159.

13 H. Mustu, H. Arbag, S. Yasyerli, N. Yasyerli, G. Dogu and T. Dogu, *Nanotechnology: Advanced Materials, CNTs, Particles, Films and Composites*, Chapter 5: Nanomaterials for Catalysis, Nano Science and Technology Institute, Cambridge, MA, U.S.A, 2013, **vol. 1**, pp. 463-466.

14 R. Koirala, K. R. Gunugunuri, S. E. Pratsinis, and P. G. Smirniotis, *J. Phys. Chem. C*, 2011, **115**, 24804.

15 I. G. Osojnik Črnivec, P. Djinović, B. Erjavec and A. Pintar, *Chem. Eng. J.,* 2012, **207-208**, 299.

16 *(a)* M. Zawadzki, *J. Alloys and Compounds*, 2008, **454**, 347; *(b)* D. Andreeva, R. Nedyalkova, L. Ilieva and M. V. Abrashev, *Appl. Catal. A: Gen*., 2003, **246**, 29.

17 *(a)* A. Horvath, L. Guczi, A. Kocsonya, G. Safran, V. La Parola, L. F. Liotta, G. Pantaleo and A. M. Venezia, *Appl. Catal. A: Gen*., 2013, **468**, 250; *(b)* J. C. Vargas, S. Ivanova, S. Thomas, A.-C. Roger and V. Pitchon, *Catal.,* 2012, **2**, 121;

18 *(a)* C. W. Bunn, *Chemical Crystallography,* Oxford University Press, 1945*; (b)* A. B. Sifontes, M. Rosales, F. J. Méndez, O. Oviedo and Tamara Zoltan*, J. Nanomater.,* 2013, Article ID 265797, 9 pages.

19 P. Djinović, I. G. Osojnik Črnivec, B. Erjavec and A. Pintar, *Appl. Catal. B: Environ*., 2012, **125**, 259.

20 *(a)* D. Sangeeta and J. R. Lagraff, *Inorganic materials chemistry desk reference*, CRC Press, 2005, ISBN 978-0-8493-0910-6, p. 103; *(b)* BS 1377: Part 2(8), *Determination of particle density, Methods of Test for Soils for Civil Engineering Purposes*, Classification Tests, British Standards Institution, London, 1990.

21 A. K. Zhou, X. Wang, X. Sun, Q. Peng and Y. Li, *J. Catal*., 2005, **229**, 206.

22 N. W. Hurst, S. J. Gentry, A. Jones and B. D. McNicol, *Catal. Rev. Sci. Eng.,* 1982, **24**, 23.

23 P. Kumar, Y. Sun and R. O. Idem, *Energy Fuels,* 2008, **22**, 3575.

24 J.-W. Snoeck and G. F. Froment, *Ind. Eng. Chem. Res*., 2002, **41**, 4252.

25 V. M. Gonzalez-Delacruz, R. Pereniguez, F. Ternero, J. P. Holgado and A. Caballero, *ACS Catal.,* 2011, **1**, 82.

26 (*a*) L. Shi, G. Yang, K. Tao, Y. Yoneyama, Y. Tan and N. Tsubaki, *Acc. Chem. Res*., 2013, **46**, 1838; (*b*) L. C. S. Kahle, T. Roussiere, L. Maier, K. H. Delgado, G. Wasserschaff, S. A. Schunk and O. Deutschmann, *Ind. Eng. Chem. Res.,* 2013, **52**, 11920.

27 A. Donazzi, A. Beretta, G. Groppi and P. Forzatti, *J. Catal.,* 2008, **255**, 241.

28 A. Erdohelyi, J. Cserenyi and F. Solymosi, *J. Catal.,* 1993, **141**, 287.

29 J. M. Wei and E. Iglesia, *J. Catal*., 2004, **225**, 116.

30 T. E. Solh, K. Jarosch and H. de Lasa, *Ind. Eng. Chem. Res.,* 2003, **42**, 2507.

31 (*a*) L. B. Avdeeva, T. V. Reshetenko, V. B. Fenelonov, A. L. Chuvilin and Z. R. Ismagilov, *Carbon,* 2004, **42**, 2501; (*b*) C. D. Tan and R. T. K. Baker, *Catal. Today,* 2000, **63***,* 3; (*c*) J. Li, G. Lu, K. Li and W. Wang, *J. Mol. Catal. A: Chem.,* 2004, **221**, 105.

32 D. Duprez, M. C. Demicheli, P. Marecot, J. Barbier, O. A. Ferretti and E. N. Ponzi, *J. Catal.,* 1990, **124**, 324.
33 K. Li, H. Wang, Y. Wei and D. Yan, *Int. J. Hydrogen Energy,* 2011, **36**, 3471.
34 H. Liang, J. M. Raitano, G. He, A. J. Akey, I. P. Herman, L. Zhang and S.-W. Chan, *J. Mater. Sci.,* 2012, **47**, 299.